The Impact of Historical Land-Use Changes on the Near-Surface Atmospheric Conditions on the Swiss Plateau

Nicolas Schneider

Institute of Geography, University of Bern, Bern, Switzerland

Werner Eugster

Institute of Geography, University of Bern, Bern, Switzerland, and Swiss Federal Institute of Technology, Zurich, Switzerland

Barbara Schichler

Institute of Geography, University of Bern, Bern, Switzerland

Received 12 August 2003; accepted 16 November 2003

ABSTRACT: The effects of historical land-use changes on the Swiss Plateau on the near-surface atmospheric conditions of typical summer days in July were investigated in a case study. A mesoscale dynamical nonhydrostatic model with a horizontal resolution of 1 km^2 was used. Two simulations of historical (around 1850) and present conditions as well as six sensitivity experiments were conducted in order to assess the importance of changes in the physiological, morphological, and soil properties. The modeled daily average

Corresponding author information: Nicolas Schneider, Climatology and Meteorology, Institute of Geography, University of Bern, CH-3012 Bern, Switzerland.
E-mail address: schneid@giub.unibe.ch

temperature was 0.25°C lower under present than past land-use conditions. During the day, changes in temperature showed a heterogeneous spatial pattern that depended on the type of the land-use conversion and its geographic location. In areas where afforestation took place, an average warming of more than 1.0°C was observed. In contrast, deforestation resulted in a cooling of up to 2.0°C. Furthermore, an average increase in the water vapor mixing ratio of 0.2 g kg^{-1} was simulated during the day. During the night, the average temperature was up to 0.6°C lower under present land-use conditions. This nighttime cooling is mainly restricted to low-lying areas on the formerly frequently inundated plains. The diurnal temperature range in the area of land-use changes increased by 0.1°–0.3°C. The sensitivity experiments showed that the daytime temperature decrease was mainly caused by morphological changes, while the altered physiological properties are the dominant factor for the nighttime cooling. The water vapor mixing ratio during the day was mainly affected by changes in the physiological properties.

KEYWORDS: Mesoscale modeling; Landscape change; Land–atmosphere exchange

1. Introduction

In the context of global warming, a better understanding of the effects of land surface changes on the climate has become more and more important in order to be able to separate the impacts of land-use changes on the regional climate from those of global warming. Stohlgren et al. (Stohlgren et al., 1998), for example, concluded that, on a regional scale, larger-scale temperature changes associated with observed increases in greenhouse gases may be dominated by the effects of land-use practices on the climate. Similar results were found by Chase et al. (Chase et al., 2001), who showed that simulated near-surface temperature anomalies originating from historical observed CO_2 concentrations combined with aerosol forcing and simulated temperature anomalies originating from the direct and remote effects of historical, anthropogenic land-cover changes are of similar magnitude. A decade ago, Pielke and Avissar (Pielke and Avissar, 1990) concluded that an adequate assessment of climate change cannot be achieved unless mesoscale landscape characteristics and their changes over time can be accurately determined. Yet, knowledge about the effects of land-use changes on weather and climate on the meso-β scale is still very limited.

Mölders (Mölders, 1999) examined the impact of drainages of marshes and water meadows on the local atmosphere. She showed that surface temperatures over marshland were up to 2°C higher than over grassland at noon. Consequently, the enhanced sensible heat fluxes contributed to slightly higher air temperatures over marshland than over grassland in the afternoon.

In a subsequent study, she investigated the effects of a set of land-use changes (deforestation, urbanization, afforestation, recultivation of open-pit mines, drainage) on atmospheric processes during a typical day in May (Mölders, 2000). The results indicated that areas dominated by grassland and forests are more sensitive to concurrent land-use changes than are predominantly agriculturally used areas.

Table 1. Experiments carried out in this study.

Name	Description
LU19	Past land use in area of land-use changes due to JGK without present land use
LU20	Present land use
PHYS	As in LU19, but physiological properties as in LU20
MORPH	As in LU19, but morphological properties as in LU20
SOIL	As in LU19, but soil properties as in LU20
M-S	As in LU19, but morphological and soil properties as in LU20
P-S	As in LU19, but physiological and soil properties as in LU20
P-M	As in LU19, but physiological and morphological properties as in LU20

Venäläinen et al. (Venäläinen et al., 1999) examined the influence of peatland draining with subsequent afforestation on the local climate in Finland. They found that minimum temperatures in August were lower than before in the heavily drained regions.

In our case study, we report on the effects that historically documented anthropogenic land-use and land-cover changes on the Swiss Plateau impose on the near-surface atmospheric conditions of typical days in summer. Most of the landscape transformations in the study area occurred in the nineteenth century after the leveeing and draining of the formerly marshy and frequently inundated plains had started in 1869. The type of land-use and land-cover change as seen on the Swiss Plateau is considered a typical example of landscape transformation as it occurred in many industrialized countries (see also Galler et al., 2003). So as to be able to distinguish changes in the atmosphere occurring as a consequence of the historically documented land-use changes in the study area from extrinsic effects, the concurrent external forcing factors such as the radiative forcing of CO_2 and other trace gases, and the solar flux were kept unchanged.

2. Model, study area, and data

The three-dimensional atmospheric Meteorology and Photochemistry Model (MetPhoMod) (Perego, 1996; Perego, 1999) was used in its nonhydrostatic mode. Two simulations accounting for the different types of land use (past and present land use) and six sensitivity runs were carried out (Table 1). The period chosen for simulation was from 0000 local time (LT) 4 July 1998 to 0600 LT 6 July 1998, a period that can be considered as typical summer fair-weather days (Fig. 1). Another important reason for the choice of this simulation period was the availability of an extensive set of field measurements, which was used for model validation (see section 3.1.). In order to allow the model to spin up, the first 6 h of the simulation runs were not analyzed in this study.

While the atmospheric input data for the top and lateral boundaries prescribed to the model (see section 2.6.) were identical for all simulations, the physical properties of the soil and the surface were adjusted to represent the particular land use of each simulation. Additionally, all simulations were initialized with the same vertical profile of virtual potential air temperature, horizontal wind speed, and water vapor mixing ratio as well as identical ground and surface temperatures.

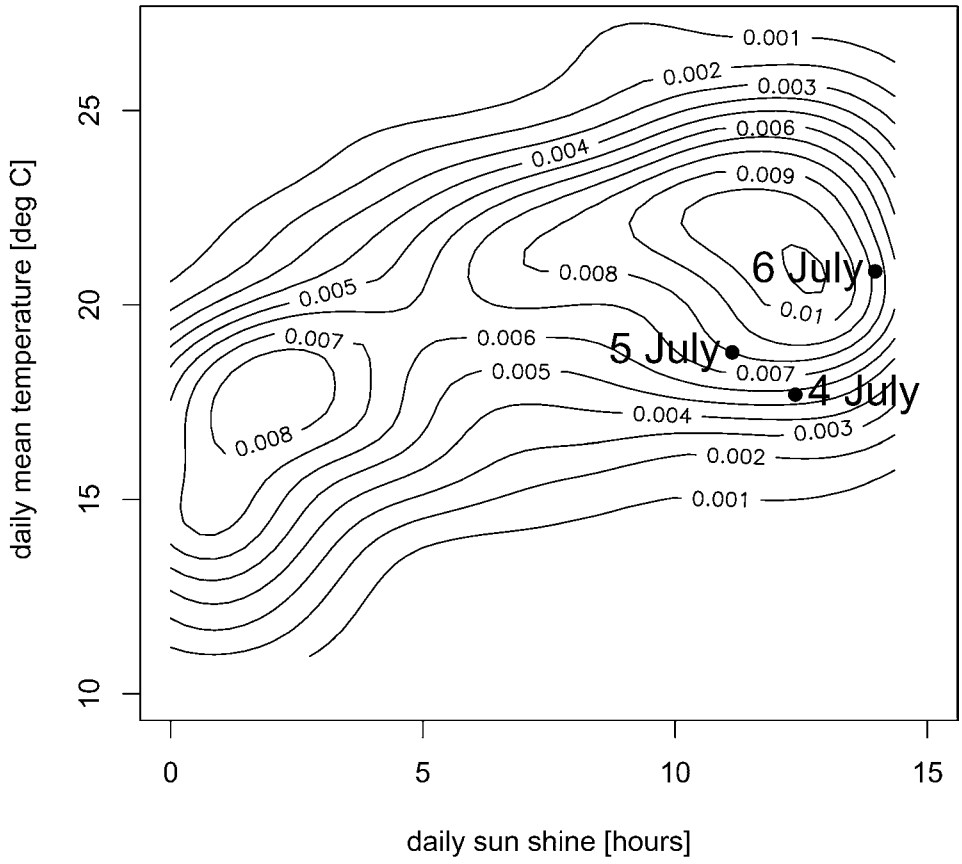

Figure 1. Two-dimensional density distribution of daily mean temperature and daily sum of sunshine hours for all days in Jul from 1978 to 2003 at Neuchâtel (see Fig. 2). The three days from 4 to 6 Jul 1998 lie very close to the most frequent combination of daily mean temperature and daily sum of sunshine hours. The most frequent combinations are those days with a daily sum of sunshine hours of about 12–13 h and a daily mean temperature of more than 20°C, i.e., essentially clear-sky days.

Consequently, the influence of the large-scale climate over the 150 yr was kept constant, which allowed the quantification of the near-surface atmospheric changes that resulted from the anthropogenic land surface changes only.

2.1. Brief description of the model

MetPhoMod, a three-dimensional, Eulerian, prognostic model for the calculation of nonhydrostatic mesoscale meteorology and atmospheric chemistry was used. A detailed description of the model can be found in Perego (Perego, 1996; Perego, 1999, and online at http://www.giub.unibe.ch/klimet/metphomod/). The main features relevant for this study are briefly described below.

MetPhoMod uses a Cartesian grid with regular and underground grid points, which makes it a particularly suitable tool for simulations in very complex terrain

as it requires no smoothing of the topography. This is considered an advantage for model applications in Switzerland.

Atmospheric turbulence was parameterized by using a k–ε turbulence closure scheme (Apsley and Castro, 1997), which includes prognostic differential equations for the turbulent kinetic energy and the turbulence dissipation rate ε. Advection is calculated with the use of the parabolic piecewise method (PPM) of Colella and Woodward (Colella and Woodward, 1984). Additionally, a correction method by Clappier (Clappier, 1998) is applied to avoid over- and undershooting produced by the time-splitting approach. The model does not include a convective parameterization as it is not required at the high resolution used in this study, which can resolve larger convection cells. Clear-sky parameterizations for the solar radiation (Paltridge and Platt, 1976) and for IR radiation (Pielke, 1984) were used.

The five-layer soil module with lower bounds of the layers at depths of 0.04, 0.16, 0.36, 0.64, and 1.0 m below the surface consists of a prediction equation for the soil temperature as a function of depth z:

$$\frac{\partial T_G(z)}{\partial t} = k_s \frac{\partial^2 T_G(z)}{\partial z^2}, \tag{1}$$

where $T_G(z)$ is the ground temperature at depth z, and k_s is the thermal diffusivity of the soil. The temperature of the lowest ground layer was kept constant during the model run and was set to the annual mean temperature. For the calculation of ground temperatures and heat fluxes, thermal diffusivity was assumed to be constant.

The plant module is based on the big-leaf–big-stoma approach by Deardorff (Deardorff, 1978), including a simple physiological response of stomatal openings to the incoming shortwave radiation. It consists of solving a heat balance equation for a single canopy layer and for the surface. The energy balance equation for the canopy considers sensible and latent heat flux exchanges with the surrounding air in addition to the shortwave and longwave radiation fluxes.

A strategy of dominant land use was used to determine the single type of vegetation in a grid cell. Additionally, the vegetation fraction indicates the part of the grid cell that is covered by vegetation. Due to the small size of the cells (1 km^2; see section 2.3.), the heterogeneity of the land use in the study area was adequately represented.

2.2. Study area

Most of the study area is located on the Swiss Plateau. It comprises three major lakes and is nowadays one of the most important agricultural areas in Switzerland. Until the beginning of the nineteenth century, the plain around the three lakes was frequently inundated and blanket bogs were dominant. In the central area between the three lakes, a blanket bog area of approximately 400 km^2 existed. Its agricultural use was limited to infrequent harvesting of hay and litter.

In the second half of the nineteenth century, a major civil engineering project called Juragewässerkorrektionen (hereafter JGK) was initiated to adjust the lake and river system. The courses of the major rivers were straightened, diverted to the lakes, or replaced by new canals. Existing canals between the lakes and the outflow

of the last lake in this system were enlarged. Subsequently, much of the low-lying plains were drained and the mean levels of the three lakes were lowered by 2.5 m; the large blanket bog area between the lakes was converted into intensively used agricultural land. In 1994, the current land use was determined for a 96.1-km^2 subdomain using a multispectral–multitemporal analysis of four *Landsat-5* Thematic Mapper (TM) scenes (Eugster et al., 1998). The land use was 45.2% arable lands, 32.7% forests and woodlands, 12.4% lakes and rivers, 6.9% urban areas and infrastructure, and 2.8% unclassified land. The arable land consisted of 62.2% meadows and pastures, 15.9% cereals, 11.4% maize, 4.5% sugar beets, 2.5% orchards, 1.3% vineyards, 1.1% potatoes, and 1.1% other agricultural crops.

The soils in the area of interest are either organic peat soils in the formerly inundated plain with blanket bogs or mineral soils on the hills around the blanket bog area. The peat soils near Kerzersmoos, Switzerland, can be up to 100–200 cm in depth, with a depth to water table of typically 60–70 cm (Peyer, 1985). Near the surface an organic content of 40%–50% is typical, while lower soil layers still may contain 50%–80% organic matter (Peyer, 1985). The mineral soils only contain 3%–4% organic matter in the tilled topsoil, and soils are well developed over the 60–100-cm depth with slightly acidic to neutral pH.

2.3. Model domain

The inner model domain generously encloses the area where land-use changes due to the JGK occurred (Figure 2). The Jura Mountains constitute the northwestern border of the model domain, while the southern border reaches into the Alps. The extent of the rectangular model domain is 150 km × 80 km, and it is rotated counterclockwise by 35° from the north in order to align its longer dimension with the prevailing wind direction during this study.

The horizontal grid resolution for atmospheric, land surface, and soil grid cells is 1 km^2. The vertical resolution decreases logarithmically from 25 m at the lowest topographic elevation (425 m ASL) to 1600 m at the model top at a height of 7.8 km.

The topography of the model domain inside Switzerland was derived from a 100-m digital elevation model and from the United States Geological Survey's (USGS's) global topographic digital elevation model (GTOPO30) elsewhere. The same topography was used for all simulations assuming that the effects of changes in topographic elevation due to historical land-use changes are negligible in this particular context.

2.4. Land-use and soil data

The present land-use types inside Switzerland were taken from the Swiss National Land Census database collected between 1979 and 1985 at a resolution of 100 m × 100 m, which was aggregated to a resolution of 1 km × 1 km through the assignment of the dominant land-use type. The present land-use classification used for Switzerland consists of 24 classes, of which 19 occurred in the study domain. Twice, two classes were lumped to one single class as there was no reason for defining different soil and surface parameters for these classes, resulting in a total of 17 present land-use classes in the Swiss part of the study area.

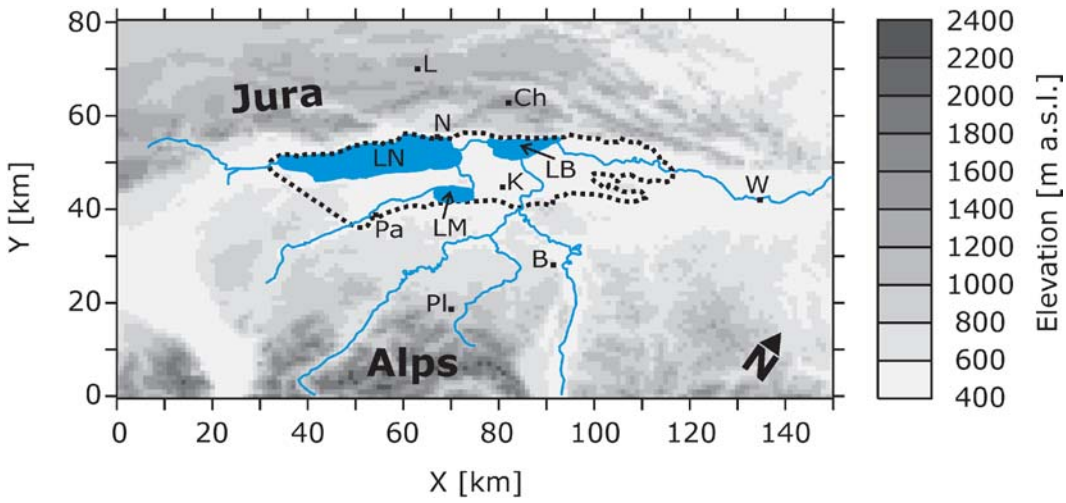

Figure 2. Topography of the study area. The extent of the domain is 150 km × 80 km with a grid resolution of 1 km^2. The three-lake region is situated between the Jura Mountains in the northwest of the domain and the Alps in the south. The broken line denotes the extent of the study area, within which past land use was reconstructed from historical maps. This corresponds approximately to the area that was influenced by the land-use conversions during the JGK. Major lakes and rivers within the domain are drawn in blue. Designated meteorological stations in the text are Bern-Liebefeld (B), Chasseral (Ch), Kerzersmoos (K), La Chaux-de-Fonds (L), Neuchâtel (N), Payerne (Pa), Plaffeien (Pl), and Wynau (W). Lakes: Lake of Neuchâtel (LN), Lake of Biel (LB), and Lake of Murten (LM).

For the model domain outside Switzerland, the USGS Global Land Cover Characteristics database version 2.0 (available online at http://edcdaac.usgs.gov/glcc/glcc.html) with 17 classes corresponding to the International Geosphere–Biosphere Programme's (IGBP's) land-cover legend was used (Loveland et al., 2000). These land-cover data have a resolution of 1 km^2. Six of these land-cover classes did not occur in the model domain. Of the remaining 11 classes, 10 corresponded directly to one of the 17 present land-use classes used for the Swiss part of the model domain. Thus, only one additional present land-use class had to be introduced, resulting in a total of 18 present land-use classes for the whole study area (Figure 3).

For the reconstruction of the land use before the JGK, historical maps originating from the period 1800–50 were used. Past land use was only reconstructed in the area where the JGK had directly affected the landscape characteristics (Figure 2). For the reconstruction of the past land use, eight land-use classes were distinguished (Figure 3). Of the past land-use classes, four corresponded directly to one of the present land-use classes. Hence, only four additional land-use classes had to be introduced to represent the past land use, giving a total of 22 classes to represent the past and present landscape characteristics of the whole study area.

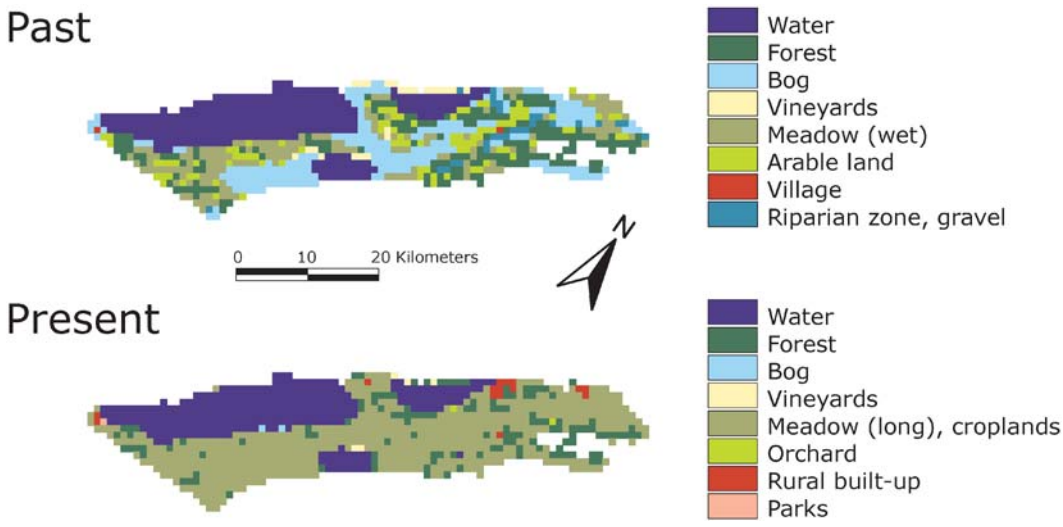

Figure 3. Past (LU19) and present (LU20) land use in the three-lake region. For clarity, the 18 present land-use classes were simplified to eight classes in this figure.

In order to minimize potentially confounding effects from the land-use changes that are not related to the JGK, past land use outside the area of direct landscape transformation was kept unchanged in all model simulations by assuming present land use. Another important reason for the assumption of present land use outside the JGK area was the lack of high quality surface cover information for the nineteenth century.

The soil properties were derived from the dominant land-use type of each grid cell. This approach assumes that soil properties and vegetation and hence the type of land use are strongly correlated. This approach is supported by the fact that this study compares two time points roughly 150 yr apart, which we believe to be sufficient to develop a new equilibrium between soil properties and vegetation. The physical parameters for the soil module of the model were assigned to the land-use classes via the use of a lookup table (Table 2) in the same way as was done in the studies by Mölders (Mölders, 1999; Mölders, 2000).

2.5. Synoptic situation

On 3 July, a frontal system passed eastward over Switzerland. At the model start, Switzerland was in the upstream area of a midtroposphere trough with northwesterly winds. The surface air pressure field indicated that the study area was under the influence of a high pressure system reaching the Alps. On the eastern side of the high pressure system, air masses were diverging. Hence, the midtroposphere postfrontal subsidence and the diverging air masses in the region of maximum subsidence led to a rapid clearing up during the night. Conditions hereafter were very clear with only few remaining clouds in the mornings of the simulated days.

Table 2. Surface and soil parameters used by the MetPhoMod model: Z_0, surface roughness length; LAI, leaf area index; α_p, plant albedo; σ_f, vegetation fraction; r_c, canopy stomatal resistance; α_s, soil albedo; ε_s, emissivity of the soil; k_s, thermal diffusivity of the soil; and c_p, specific heat capacity of the soil. The emissivity of the vegetation was assumed to be constant (0.98).

Land-use class	Z_0 (m)	LAI ($m^2\ m^{-2}$)	α_p (—)	σ_f (—)	r_c ($s\ m^{-1}$)	α_s (—)	ε_s (—)	k_s ($10^{-6}\ m^2\ s^{-1}$)	c_p ($10^6\ J\ m^{-3}\ K^{-1}$)
Mixed forests	3.0	4	0.15	0.95	120	0.175	0.975	0.70	2.5
Open forests*	2.0	4	0.15	0.80	120	0.175	0.975	0.70	2.5
Evergreen needleleaf forest*	8.0	12	0.10	0.90	200	0.175	0.975	0.70	2.5
Shrublands*	0.5	1.5	0.15	0.50	120	0.175	0.975	0.70	2.5
Vineyards	0.2	1.8	0.20	0.70	110	0.20	0.96	0.50	2.1
Orchards*	0.5	2	0.20	0.70	110	0.20	0.96	0.62	2.5
Meadow (long), croplands*	0.05	4	0.25	0.80	90	0.18	0.96	0.56	2.1
Meadow (short)*	0.01	4	0.26	0.80	100	0.25	0.96	0.56	2.1
Meadow (wet)**	0.07	3	0.16	0.80	100	0.25	0.96	0.74	2.9
Arable land**	0.05	3	0.00	0.00	0	0.18	0.96	0.70	2.5
Pasture (elevated zone)*	0.07	4	0.00	0.00	0	0.18	0.96	0.56	2.1
Lakes	0.001	0	0.18	0.80	50	0.09	0.95	0.14	4.186
Rivers*	0.01	0	0.00	0.00	0	0.09	0.95	0.14	4.186
Riparian zone, gravel**	0.5	1.5	0.00	0.00	0	0.20	0.98	0.84	2.1
Bog	0.15	2	0.26	0.15	100	0.10	0.98	0.12	3.1
Nonvegetated*	0.01	0	0.00	0.15	100	0.30	0.98	1.40	0.753
City*	1.0	0	0.00	0.00	0	0.15	0.95	1.00	2.0
Village**	0.8	4	0.00	0.00	0	0.20	0.90	1.00	2.0
Urban built-up*	0.6	4	0.26	0.30	100	0.15	0.95	1.00	2.0
Parks*	0.05	0	0.16	0.80	70	0.18	0.97	0.74	2.9
Road area*	0.01	0	0.25	0.80	90	0.15	0.96	1.00	2.0
Railway area*	0.02	0	0.15	0.50	50	0.15	0.96	1.00	2.0

* Only present land use (LU20)
** Only past land use (LU19)

2.6. Boundary conditions and initial data

The border data for the simulations with different land-use conditions were generated by nesting the inner model domain, which encloses the area of interest, in an outer domain with a coarser grid resolution. The outer domain stretches from 45°–48°N to 5°–11°E and was composed of 47 × 34 cells with a mesh size of 10 km and 25 vertical layers. For the initialization and the top and lateral boundary conditions of the coarse grid, virtual potential temperature, horizontal wind speed, and water vapor mixing ratio were taken from 6-hourly National Centers for Environmental Prediction–National Center for Atmospheric Research (NCEP–NCAR) reanalysis data with a resolution of 2.5° × 2.5° (Kalnay et al., 1996; Kistler et al., 2001). The outer model was used to generate 1-hourly boundary data for the inner model domain.

Furthermore, the inner model was initialized with the measured vertical profile of virtual potential temperature, horizontal wind, and water vapor mixing ratio

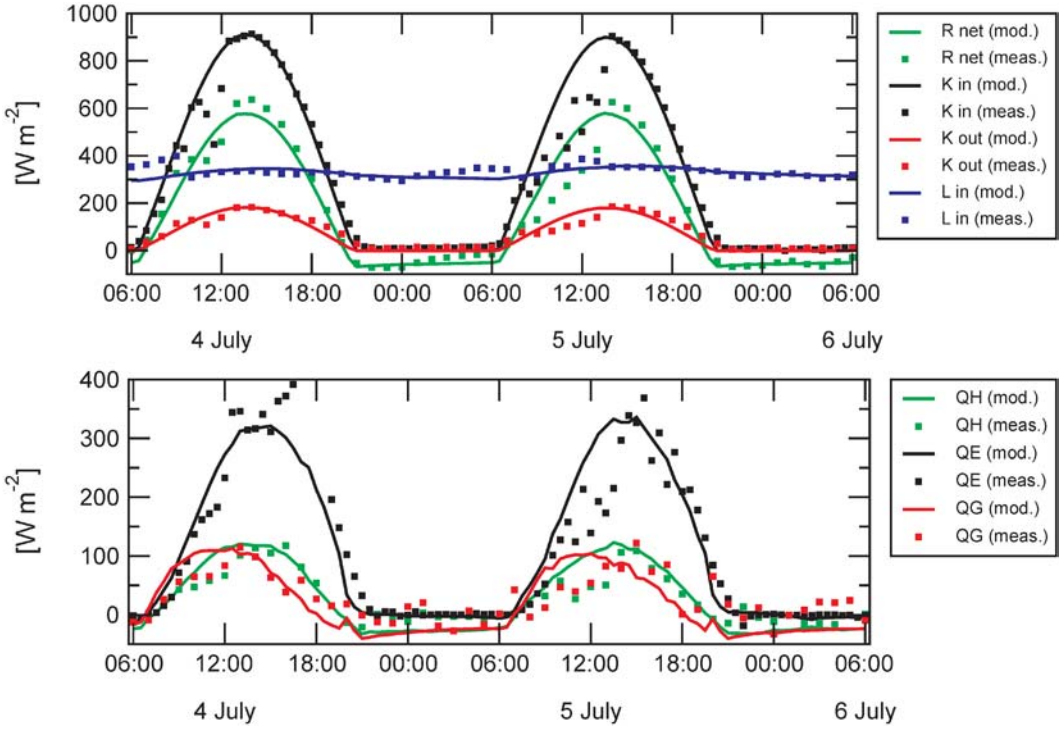

Figure 4. Comparison of measured and simulated surface energy fluxes at Kerzersmoos. The squares show values measured every 30 min at Kerzersmoos (cf. Figure 2). The solid lines show the simulated radiation components for the grid cell nearest to Kerzersmoos. (top) Net radiation (R_{net}), global radiation (K_{in}), reflected shortwave radiation (K_{out}), and incoming longwave radiation (L_{in}). (bottom) Sensible heat flux (Q_H), latent heat flux (Q_E), and ground heat flux (Q_G).

taken from balloon soundings at Payerne, Switzerland (see Figure 2) at 0000 LT 4 July 1998**.** Apart from the sounding data at model start, no other sounding data were used to drive the model. Thus, the further soundings measured at noon and at midnight of the simulated days could be used for validation purposes.

3. Agreement between model and measurements

Field measurement data from a field experiment carried out at Kerzersmoos by Siegrist (Siegrist, 2001), from seven sites of the Swiss Meteorological network (Anetz), and from twice daily rawinsonde soundings at Payerne (not shown) were used to validate the simulation with present land-use conditions (LU20). For the locations of the measurement sites, see Figure 2.

3.1. Kerzersmoos

Figure 4 (top panel) compares the diurnal variation of the radiation budget components measured at Kerzersmoos with the corresponding simulated terms of

the nearest model grid cell. The simulated reflected shortwave radiation and the net radiation were adjusted for differences in the albedo of the local surface and the average of the nearest grid cell.

In general, a very good agreement between measured and calculated radiation fluxes was found. Nevertheless, some small discrepancies occurred that were caused by three different processes. First, a few altocumulus and cirrus clouds were observed in the morning of the second day (Siegrist, 2001). As these types of clouds are not incorporated in the model, they were not represented in the simulated values. Thus, lower global radiation and higher incoming longwave radiation were simulated, resulting in a simulated net radiation differing from the measured net radiation in the morning of the second day. Second, the measured net radiation in the second half of the night from 4 to 5 July slightly differed from the simulated values. The reason for this was dew formation on the net radiometer sensor (Siegrist, 2001, pp. 31, 46). Third, the measured emitted longwave radiation was higher than simulated, which resulted in slightly overestimated maximum daily net radiation fluxes. This higher emitted longwave radiation (not shown) was caused by the difference between the soil and surface properties used for the entire model grid cell and the local conditions at the measuring site.

Figure 4 (bottom panel) shows the validation for sensible (Q_H), latent (Q_E), and ground heat flux (Q_G) at Kerzersmoos. Simulated and measured latent heat fluxes agree very well, showing only some differences in the maximum value on the first day of the simulation. An acceptable correspondence between simulated and measured values was also found for the ground heat flux. Although simulated nighttime values seem slightly lower, they were found to be very reasonable as the measurement of the ground heat flux is subject to considerable experimental uncertainty. Furthermore, the measured ground heat flux represents a much smaller area than the simulated one, which accounts for an entire grid cell. The simulated sensible heat flux was in very good agreement with measured values during the day. However, modeled nighttime values showed a rather constant negative offset of about 15 W m^{-2} compared to the measurements. At night, the model produced slightly too stable atmospheric conditions.

3.2. Swiss meteorological network stations

The agreement between the LU20 simulation and measurements from the Swiss meteorological network (Anetz) is shown in Figure 5 for two selected sites (Bern-Liebefeld and Neuchâtel, Switzerland). Simulated temperatures at Bern-Liebefeld corresponded well with measured values, while some discrepancy was found during the night at Neuchâtel. There, starting at 1900 LT, the simulated cooling rate was considerably lower than measured until around midnight. After that, simulated and measured temperatures show similar cooling rates. This discrepancy seems to be a result of the downslope cold air drainage flow from the Jura Mountain range. This cold airflow starts in the early evening but is not fully captured with the current model resolution. In this context, the characteristic topographic location of Neuchâtel station is very important: it is located on the rather steep south exposed slope of the Jura Mountain range. Although the onset of downslope cold air drainage flow at around 1700 LT (seen clearly in the V wind

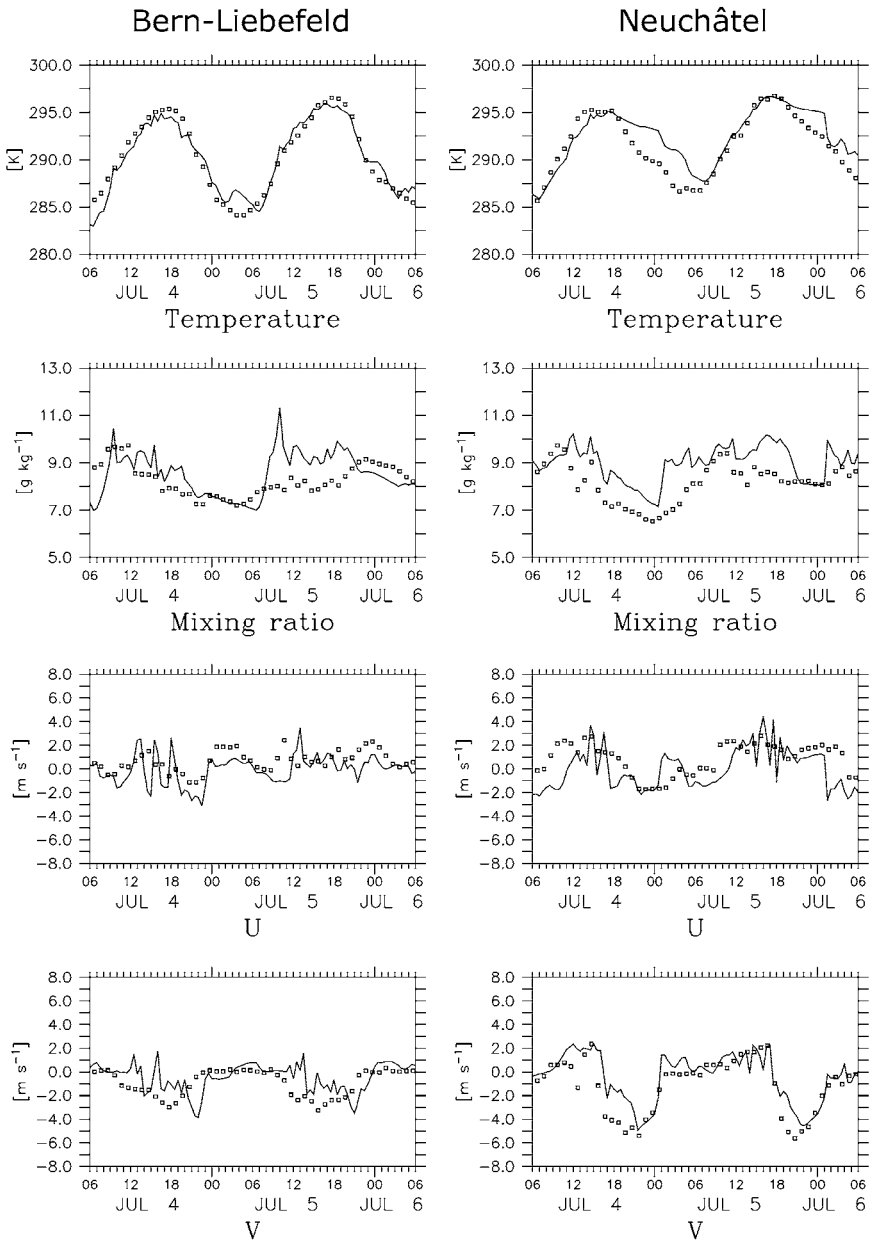

Figure 5. Comparison of measured (open squares) and simulated (solid line) absolute temperature, water vapor mixing ratio, and horizontal wind at Bern-Liebefeld and Neuchâtel. The measurements are compared with the simulated values of the grid cell nearest to the measuring site. Measurement heights for temperature and mixing ratio are 2 m above ground, while the wind is measured at 10 m above ground. Simulated values are at the lowest layer above ground (12.5 m). Wind directions (*U*, *V*) are parallel to the domain borders (cf. Figure 2).

component becoming negative in the lowest right panel of Figure 5) is well represented by the model, its magnitude is underestimated between 1700 and 2100 LT. After 2100 LT the model agrees quite nicely again with the measured V wind component. Good agreement was also found for the water vapor mixing ratio and the horizontal wind at both stations. Analysis of the horizontal wind components further showed that many (though not all) local effects—for example, the channeling effects during the day at Bern-Liebefeld—were captured nicely by the model due to its very high resolution.

4. Differences resulting from land-use changes

The land-use changes that occurred in the study area over the past 150 yr led to a distinct decrease of surface heterogeneity (Figure 3). Two land-use types (bogs and extended riparian zones) are no longer present in the study area, and forested areas have decreased by 30%. Twelve land-use conversion types, which are each represented with at least six grid cells ($\geq$0.6% of the area), were found (Table 3); altogether they cover 95.8% of the transformed area. Two types (C and K) with 38.2% of the total area describe areas that were left unchanged by the JGK. They consist of grid cells covered either by forest or water. These two types are nevertheless included in our study in order to assess the effects from surrounding land-use changes in these unchanged areas.

The average changes of the parameter values for the whole area are rather small but can be considerable for the individual conversion types (Table 3). The overall soil albedo increased slightly by 0.005, with the replacement of water and bogs by croplands being an important factor, whereas the average plant albedo increased by 0.04. The average roughness length decreased from 0.59 to 0.41 m, which can be explained by the reduction of forested areas, whereas the increase of the average leaf area index by 0.8 was a result of the 40.5% areal expansion of cropland vegetation. The overall thermal diffusivity increased only by 4.6%, while the specific heat capacity of the soil decreased by 0.4×10^6 J m^{-3} K^{-1}, whereby the above-mentioned soil conversion was playing an important role.

4.1. Near-surface air temperature

In the first few meters above the surface, the air temperature is of special interest for human beings as well as for agriculture. Figure 6 shows the difference in the average air temperature (LU20 – LU19) at the grid cells closest to the ground. The daytime average temperature was lower by 0.1° to 0.3°C, peaking at around 1600 LT on both days. A very distinct cooling effect is observed during the nights, with the largest temperature change observed at the end of the first night when the present average temperature is more than 0.6°C lower than before the JGK. On the 2 days, the daily average temperatures near the surface were 0.2° and 0.3°C cooler in the area of direct land-use change with LU20 than with LU19. However, the temperature changes varied widely among the different land-use conversion types (Table 4).

During the day, conversions A, B, and L reveal a warming of the atmosphere, while a cooling of the atmosphere is observed for conversions E, G, I, and J. Thus,

Table 3. Land-use conversion types that occurred in the study area. The differences in the model input parameter values are given for the parameters listed in Table 2. Only conversion types that are represented with six grid cells or more were considered. The differences in the model input parameter values (present–past) for the specific conversion types are shown. The area-weighted average difference denotes the mean change of the specific parameter for the whole area of land-use change. Long dashes indicate zero differences.

Conversion type	Areal fraction (%)	Past land use	Present land use	Resulting difference (present–past) in model parameters								
				Z_0 (m)	LAI ($m^2\ m^{-2}$)	α_p (—)	σ_f (—)	r_c ($s\ m^{-1}$)	α_s (—)	ε_s (—)	k_s ($10^{-6}\ m^2\ s^{-1}$)	c_p ($10^6\ J\ m^{-3}\ K^{-1}$)
A	0.7	Bog	Forest	2.85	2.0	−0.03	0.15	70	0.075	−0.005	0.58	−0.6
B	0.8	Vineyards	Forest	2.80	2.2	−0.05	0.25	10	−0.025	0.015	0.20	0.4
C	9.2	Forest	Forest	—	—	—	—	—	—	—	—	—
D	15.3	Meadow (wet)	Meadow (long)	−0.02	1.0	0.09	—	20	−0.07	—	−0.18	−0.8
E	0.8	Water	Croplands	0.05	4.0	—	0.80	—	0.09	0.01	−3.44	−2.086
F	20.1	Bog	Croplands	−0.10	2.0	0.07	—	40	0.08	−0.02	0.44	−1.0
G	0.9	Vineyards	Croplands	−0.15	2.2	0.05	0.10	−20	−0.02	—	0.06	—
H	8.9	Arable land	Croplands	—	1.0	—	—	—	—	—	−0.14	−0.4
I	8.0	Forest	Croplands	−2.95	—	0.10	−0.15	−30	0.005	−0.015	−0.14	−0.4
J	1.8	Riparian zone/gravel	Croplands	−0.45	2.5	0.10	0.30	40	−0.02	−0.02	−0.28	—
K	29.0	Water	Water	—	—	—	—	—	—	—	—	—
L	0.6	Meadow (wet)	Rural built-up	0.53	1.0	0.10	−0.65	30	−0.1	−0.01	0.26	−0.9
		Area weighted average difference		−0.18	0.8	0.04	—	11	0.005	0.006	0.02	−0.04
	3.9	Other types of conversion										

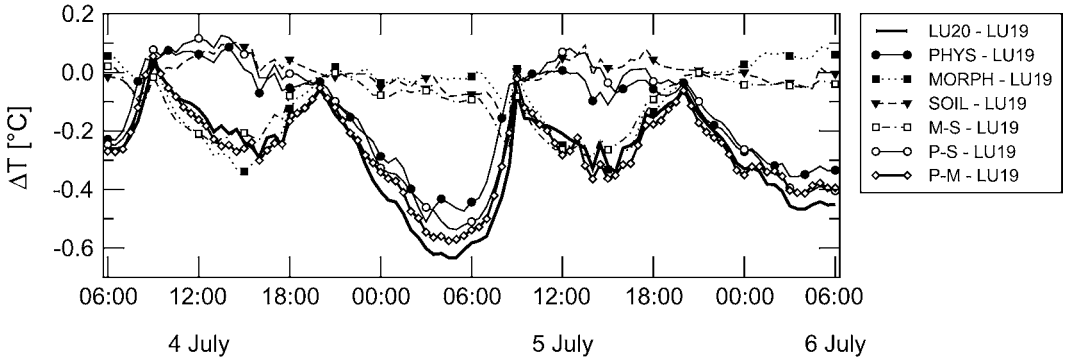

Figure 6. Differences (LU20 – LU19) in air temperature averaged over the area of land-use changes. The differences are calculated by subtracting the average temperature simulated for the past conditions (LU19) from the average temperature for the simulation with present land use (LU20) or the sensitivity experiments. For the names of the sensitivity experiments, see Table 1.

afforestation over the last 150 yr (A, B) led to an average daytime warming of more than 1.0°C (Table 4), which can be attributed to the decrease in albedo. In contrast, deforestation (I) resulted in a cooling of up to 2.0°C during the day, caused by the opposite changes in the morphological properties of the surface (albedo, surface roughness) when forested areas were replaced by croplands. A changing land cover from vineyards (G) or riparian zone (J) to croplands contributed to a cooling in the afternoon of both simulated days. For croplands, the average albedo is higher due

Table 4. Differences in near-surface air temperature at selected times (LT) for the conversion types A to L. Given is the temperature difference LU20 – LU19 (in °C). Only differences larger than the standard deviation are shown. The last column gives the difference (LU20 – LU19) of the mean daily average temperature.

Conversion type	4 Jul					5 Jul					Mean daily average
	1200	1400	1600	1700	2000	0200	0500	0900	1200	1400	
A	1.5	1.7	1.3	1.1		−1.2	−1.9	−0.9	1.4	1.5	0.0
B	1.6	1.5	0.7		−0.2	−0.8	−0.7	0.2	1.8	1.6	0.2
C					−0.1						−0.1
D					−0.1						−0.2
E				−0.4	−0.3	−1.4	−1.5	0.6			−0.5
F					−0.1	−1.1	−1.1				−0.5
G	−0.3	−0.5	−0.6		−0.1	−0.7	−0.8		−0.4	−0.5	−0.3
H						−0.5	−0.6				−0.2
I	−1.7	−2.0	−1.7	−1.3					−1.8	−2.0	−0.7
J		−0.5	−0.6			−1.5	−1.3	0.7	−0.3	−0.7	−0.5
K											−0.1
L	0.5	0.6		0.2	−0.1			−0.6	0.2	0.4	0.1

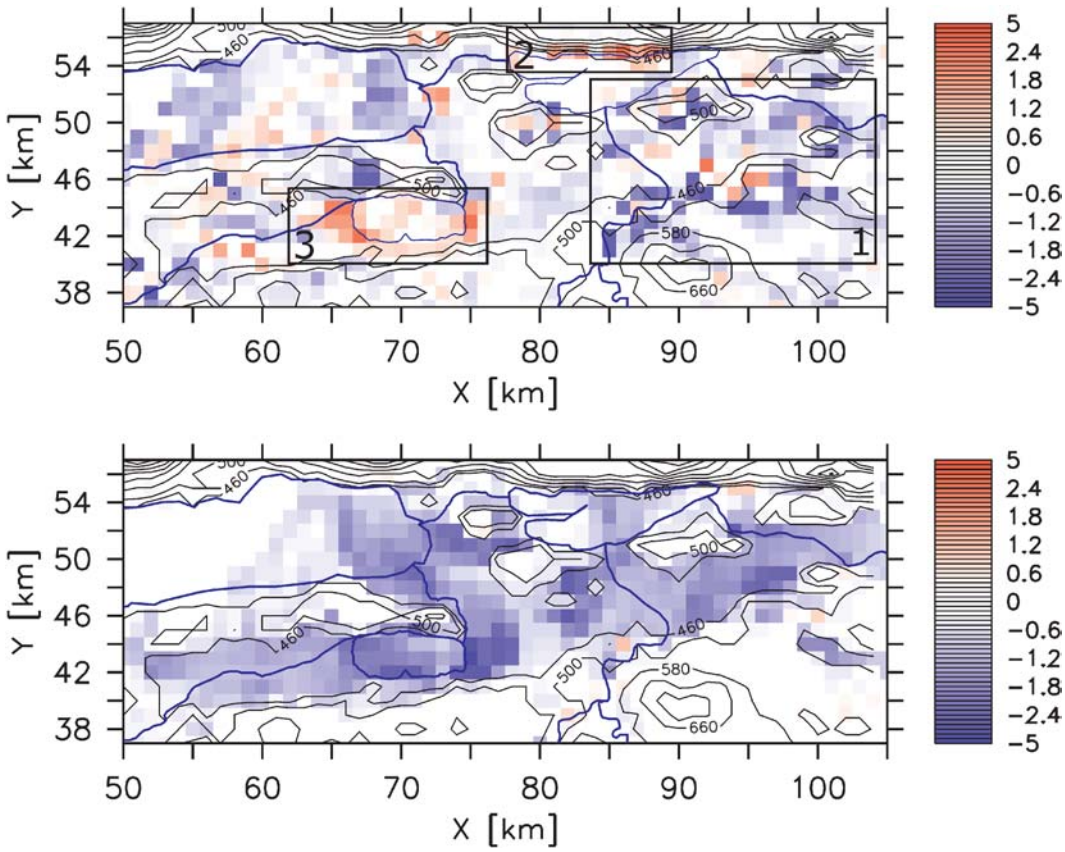

Figure 7. Difference (LU20 – LU19) in near-surface air temperature (°C) in the central part of the study domain. (top) 1400 LT 5 Jul and (bottom) 0500 LT 5 Jul. The numbered areas in the top panel denote regions mentioned in the text (cf. section 4.1.).

to a higher plant albedo and a higher vegetation fraction, while the surface roughness is lower.

A representative example for afternoon conditions in the central part of the study area is shown in Figure 7 (top panel). Three local patterns can be distinguished. First, most of the deforestation that took place occurred in the eastern part of the domain (region 1 in Figure 7). This led to a distinct cooling dominating the local atmospheric conditions. Second, warmer conditions are observed at the northern edge of the Lake of Biel, where vineyards were partly replaced by forest (region 2 in Figure 7). There, the steep topography on the southern-facing slope of the Jura Mountains leads to a very high insolation during the afternoon that in turn favors temperature changes due to altered morphological properties. Third, the local atmospheric conditions around the Lake of Murten nowadays are distinctly warmer (region 3 in Figure 7). At the western and eastern edges of the lake, land was gained as a result of the lower level of the lake after the JGK. Most of the new land is nowadays covered with forest. Furthermore, former blanket bog areas were

drained and are now either forested or used as croplands. These land-use changes resulted in higher air temperatures, favored by the absence of deforestation in this area. Additionally, the topographic situation of the lake between two hills reduces the turbulent mixing of the warmer local air masses with cooler air masses from the upstream or eastern area.

During the night, much cooler conditions were simulated for LU20 than for LU19. The difference in the average temperature for the area of direct land-use changes is monotonically increasing and peaks around 0500 LT. Several land-use conversion types contributed to the cooling effect (Table 4). In contrast to the daytime situation, afforested areas (A, B) now show a strong cooling, with a maximum cooling of up to 1.9°C for the grid cells converted from bog to forest. Areas that had once been frequently inundated (F, J), and which were converted to croplands, also show a considerable cooling. At 0200 and 0500 LT 5 July the average cooling caused by these conversions was 1.1°C. Areas that were less prone to inundation and hence formerly used as vineyards or arable land showed a weaker cooling of 0.5° and 0.6°C at 0200 and 0500 LT, respectively. Figure 7 (lower panel) shows the difference in air temperature shortly before sunrise (0500 LT 5 July). The nighttime cooling is mainly restricted to the low-lying areas with the formerly frequently inundated plains. Due to the topography, a notable cooling could only be observed up to a height of about 480 m ASL (Figure 7, bottom panel), which corresponds to about 50 m above the lowest elevations. The maximum cooling at night was 4.6°C.

The average diurnal temperature range (DTR) in the area of direct land-use changes increased by 0.1° on the first day and by 0.3°C on the second day, with maximum changes of 2.9° and 3.9°C, respectively. The daytime maximum temperatures show an analog pattern to the average temperature changes in the afternoon (Figure 7, top panel), with lower maximum temperatures in the areas of cooling and vice versa. The minimum temperatures occurring at the end of the night showed a rather uniform spatial pattern with up to 3.0°C lower minimum values under present conditions in the low-lying areas. In general, the increase in the DTR of LU20 can be attributed to the lower minimum temperatures as compared to LU19.

4.2. Energy fluxes at the surface

4.2.1. Average over area of land-use changes

Figure 8 shows the changes in the energy budget components averaged over the area of land-use changes. Energy flux differences reveal the expected diurnal variation. During the daytime, the net radiation in LU20 is distinctly lower than in LU19. The obvious reason for this is the higher average albedo in LU20 compared to LU19; there were increases in both the albedo of the soil and the plant albedo. The higher average albedo in LU20 caused a negative difference in the net shortwave radiation of up to 30 W m^{-2} compared to LU19. During the night, the average net radiation remained virtually unchanged despite the changes of the turbulent and ground heat flux components (Figure 8) involved therein. In LU20, the altered soil properties led to a lower downward ground heat flux during the day and also to a lower upward ground heat flux during the night. This can be

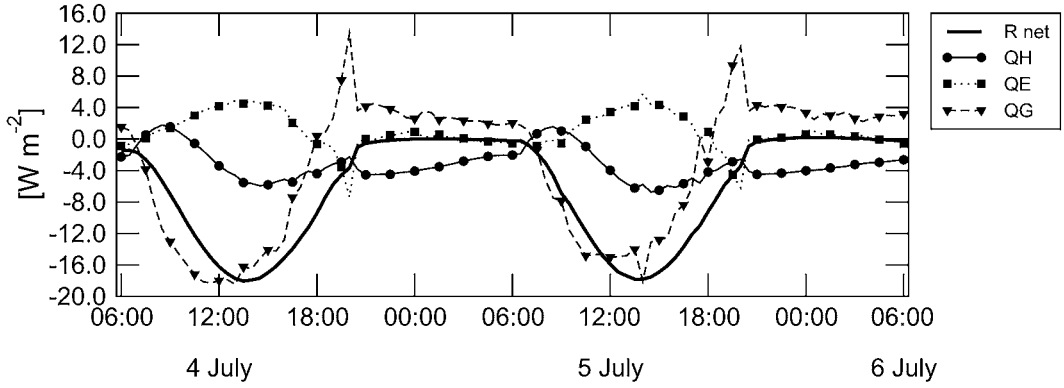

Figure 8. Differences (LU20 – LU19) in the energy budget components at the surface averaged over the area of land-use changes: R_{net} is the net radiation, Q_H is the sensible heat flux, Q_E is the latent heat flux, and Q_G is the ground heat flux.

explained by the lower net radiation in LU20 during the day and thus a smaller warming of the soil. The land-use changes also led to an altered partitioning of the incoming energy between sensible and latent heat during the day. For the present land-use conditions, the partitioning of energy is in favor for latent heat rather than sensible heat. Since more energy is released by evapotranspiration and less as sensible heat, the atmosphere is moister but cooler during the day in LU20 than in LU19. At night, the changes in the latent heat flux are negligible while a greater downward sensible heat flux was simulated in LU20 than in LU19.

4.2.2. Differences by conversion type

In order to assess the impact of the different land-use conversions on the near-surface atmospheric conditions, the radiation budget components at the surface were group averaged by conversion type. Figure 9 shows the changes in the radiation budget components (LU20 – LU19) at two relevant points in time, which are representative for the situation during the day and the night.

During the day, conversions associated with afforestation (A, B) show a positive change in the net radiation and the sensible heat flux and negative differences in the latent heat flux, while the conversion describing deforestation (I) shows the opposite. Thus, the Bowen ratio (Q_H/Q_E) increased in afforested areas and decreased in deforested areas. In both cases, the changes in the ground heat flux are rather small.

For the most abundant conversion from bog to croplands (F), the changes in the average radiation budget components seem rather small. Nevertheless, the negative changes in the net radiation and the sensible heat flux indicate a cooling effect on the atmosphere. The same cooling effect can better be seen for the conversion from riparian zone to croplands (J).

During the night, most of the conversions show a negative difference in the sensible heat flux and a positive change in the ground heat flux while changes in

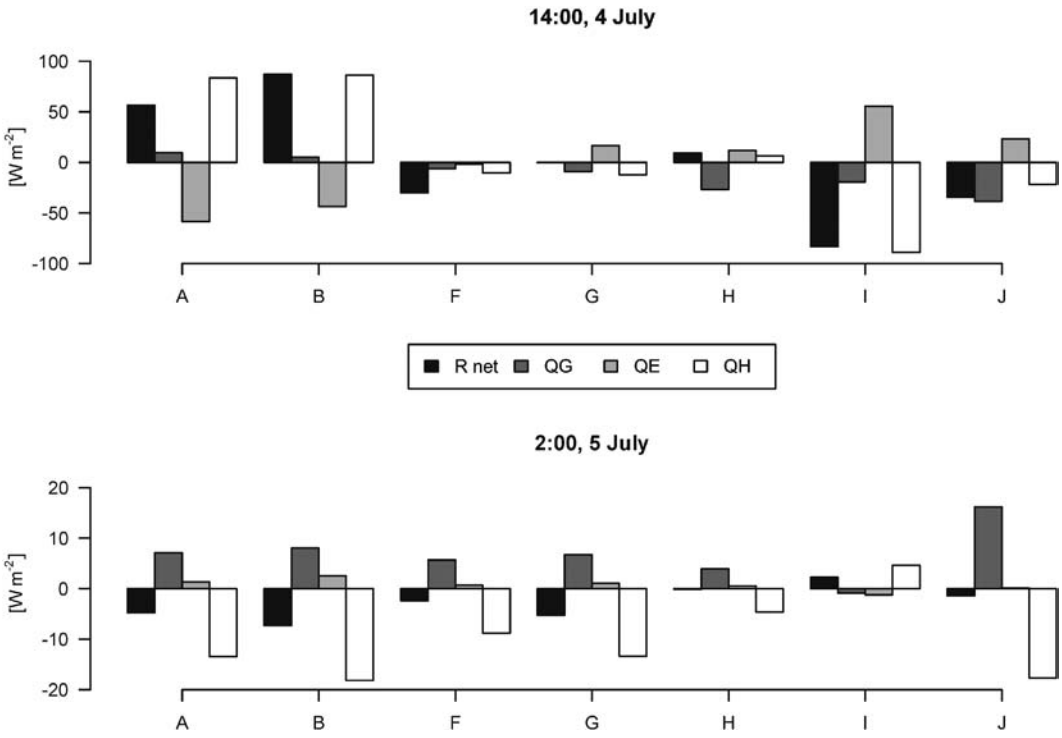

Figure 9. Average differences (LU20 – LU19) in the radiation budget components at the surface for different conversion types (cf. Table 3). The situation at (top) 1400 LT 4 Jul and (bottom) 0200 LT 5 Jul. The net radiation is denoted by R_{net}, Q_H is the sensible heat flux, Q_E is the latent heat flux, and Q_G is the ground heat flux.

the latent heat flux are generally small. Thus, most of the conversions contribute to cooler conditions in LU20 than in LU19.

4.3. Humidity

The differences in the near-surface average water vapor mixing ratio are most pronounced during the day, with an average increase of almost 0.2 g kg^{-1} (not shown). The maximum increase is observed in the morning of the second day of the simulation with 0.36 g kg^{-1}. During the night, the mixing ratio increased by 0.05 g kg^{-1} only. Although the soil water availability in LU19 was generally higher due to the marshy ground conditions on the frequently inundated plains, the total evapotranspiration was lower. The effect of the lower canopy stomatal resistance is overcompensated by the higher leaf area index used for the present vegetation. The higher transpiration of the present vegetation can best be seen in the few hours after sunrise, when the insolation rapidly increases and the increase in the mixing ratio reaches the maximum value (not shown). This increase is primarily caused by the conversion types E through J, which all describe land-use changes to croplands.

Apart from that, two conversion types differ from the average pattern: first,

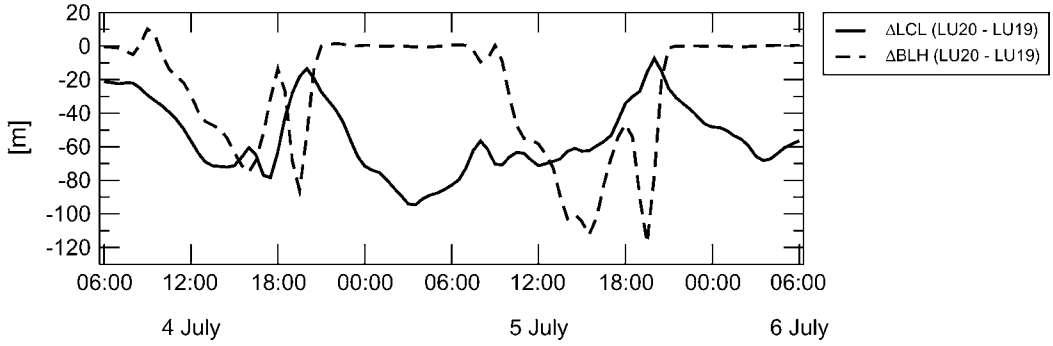

Figure 10. Differences (LU20 – LU19) in boundary layer height (BLH) and LCL averaged over the area of land-use changes. The differences are given in meters.

deforestation (A, B) led to a decrease in the mixing ratio close to the surface during the day, which can result in a locally drier atmosphere. Second, where land was gained due to the lowering of the lake levels and thereafter converted to cropland (E), a drier atmosphere was simulated from late afternoon until sunrise.

4.4. Convection

The interaction between the surface and the atmosphere plays a crucial role regarding the development of convective cells and, consequently, of cumulus convective rainfall. Any aspects of landscape characteristics that influence the heating and moistening of the atmospheric boundary layer will affect the potential for cumulus convective rainfall (Pielke, 2001).

The reduced net surface radiation balance in LU20 and the changed energy partitioning at the surface thus affected the growth of the mixed boundary layer: the lower net radiation led to lower fluxes of sensible and latent heat into the atmosphere and thus a lower entropy in the air. This led to the buildup of a shallower present boundary layer during the day, which makes up a difference of up to 100 m over the area of land-use changes (Figure 10). In addition, deep convection depends significantly on the Bowen ratio. With the smaller Bowen ratio in LU20, the thermodynamic potential for deep convection is increased (Segal et al., 1995). In agreement with that, the lifting condensation level (LCL) in LU20 is generally lower (Figure 10). Due to the lower near-surface air temperature and a similar or slightly higher mixing ratio in LU20, the air is closer to saturation and therefore the LCL is lower.

The lifted index (LI) is a good measure of stability during the warm season. It is defined as

$$\mathrm{LI} = T_{500\mathrm{mb}} - T_{p500\mathrm{mb}}, \tag{2}$$

where $T_{500\mathrm{mb}}$ is the temperature of a parcel of air lifted dry adiabatically to the LCL and then moist adiabatically up to 500 mb. Here $T_{p500\mathrm{mb}}$ is the observed temperature at 500 mb. Regarding the average of the LI over the area of land-use changes, only small negative daytime and positive nighttime differences were

found (not shown). However, on all simulated days a sharp drop of the difference in the LI (LU20 – LU19) between 0800 and 0900 LT was found, indicating a transition from slightly more stable nocturnal conditions in LU20 than in LU19 to more convective daytime conditions in the present than in the past.

5. Sensitivity studies

In order to assess the importance of changes in the specific parameter values for the changes in the near-surface atmospheric conditions, six additional sensitivity experiments were carried out (cf. Table 1). All combinations of changes in the physiological (leaf area index, canopy stomatal resistance), morphological (albedo of soil and vegetation, roughness length, vegetation fraction), and soil properties (specific heat capacity, thermal diffusivity, and ground emissivity) were simulated.

Figure 6 shows the differences in the average temperature at the lowest model level for all experiments. During the day, the experiments with altered morphological properties (i.e., MORPH) reveal a temperature decrease, while the experiments with changes in the physiological properties tend to increase the temperature. During the day, the net radiation is up to 30 W m^{-2} lower in MORPH than in LU19. The difference in the net radiation entirely originates from changes in the net shortwave radiation since the average albedo for the area of land-use conversions increased from 0.15 to 0.18, while no changes were found for the net longwave radiation. As a response to the lower net radiation, the sensible and latent heat flux decreased by up to 10 and 5 W m^{-2}, respectively, and the ground heat flux was about 10 W m^{-2} lower in MORPH than in LU19. It must be recalled that the sensible and latent heat fluxes as well as the ground heat flux are simulated at the surface, while the net radiation is simulated just above the vegetation canopy. The changes in the morphological properties led to a different partitioning of the incoming energy between sensible and latent heat flux, resulting in a lower Bowen ratio. The still abundant soil moisture allowed transpiration to proceed without the need for a stronger physiological control. Therefore, it did not significantly change the water vapor mixing ratio, but the lower sensible heat flux contributed to the cooling of the air. Moreover, the different partitioning of the incoming energy and the resulting decrease in the Bowen ratio could be found in all sensitivity experiments with altered morphology.

When only the physiological properties were changed (PHYS), the daytime net radiation increased by up to 10 W m^{-2}. In this case, no changes resulted for the net shortwave radiation, so the difference in the net longwave radiation was entirely responsible for the change in the net radiation. The incoming longwave radiation decreased by 4 W m^{-2}, while the outgoing longwave radiation was up to 14 W m^{-2} lower than compared to LU19. Hence, the combined convective losses of sensible and latent heat were enhanced in PHYS, thereby cooling the foliage and reducing the emission of longwave radiation. The average latent heat flux was up to 5 W m^{-2} greater in PHYS than in LU19, while the sensible heat flux increased by up to 3 W m^{-2}.

The experiment with changes in both the morphological and physiological properties (P-M) led to an adequate simulation of the present minus past (LU20 – LU19) daytime differences in the air temperature. This suggests that changes in the

soil properties had little or no effect on the daytime temperatures. This is also confirmed by the SOIL experiment. The changes in the water vapor mixing ratio (not shown) also indicated that the combined changes of morphological and physiological properties resulted in a nonlinear amplification of the increase in the mixing ratio. However, the daytime temperature decrease resulting from morphological changes dominated the temperature increase due to changed physiological properties. For the humidity, the higher daytime evaporation due to physiological changes is more important.

During the nighttime, the changes in the physiological properties become the dominant factor influencing the temperature. The characteristics of the LU20 – LU19 nighttime cooling can be reproduced by all sensitivity experiments that include changes in the physiological properties (PHYS, P-S, P-M) (Figure 6). The altered structure of the model canopy, which is mainly due to the higher leaf area index, leads to a changed in-canopy thermal regime. The net radiation loss from the canopy is smallest for PHYS, which leads to a smaller radiative cooling of the canopy than in LU19. As a consequence, the foliage temperature is higher than in LU19. This, in turn, leads to an increased net radiation loss above the canopy, which is comparably high during clear and calm summer nights. In order to compensate for the enhanced loss of energy by longwave radiation, the downward flux of sensible heat is greater and thus a cooling of the lowest few meters of the atmosphere results. In addition to the higher radiation loss by the warmer canopy, a lower upward ground heat flux resulted for most experiments, including LU20. The changes in the morphology and physiology also led to cooler ground conditions, which are more pronounced during the day.

6. Discussion

The results indicate that the historical land-use changes on the Swiss Plateau affected the near-surface thermodynamics in various ways. The daytime changes are distinctly influenced by the topography of the study area. Areas on the steep southern slope of the Jura Mountains as well as the area around Lake of Murten, where land was gained after the JGK, show a temperature increase. In areas with former blanket bog and peat soils, a weak cooling tendency was observed. This is in good agreement with the findings by Mölders (Mölders, 1999), who showed that air temperatures over grassland were about 0.5°C lower than over marshland in the afternoon of a typical summer day. At noon, the temperature difference was even up to –2.0°C. She explained that these changes were the results of the greater heat capacity and the lower thermal diffusivity of the soil as well as because of the lower albedo of marshland. In contrast, our sensitivity analyses showed that most of the temperature changes were initially caused by the albedo effect, whereas changes in the soil conditions were only of minor importance. However, the daytime cooling was not directly caused by the lower net radiation and the subsequent changes in the radiation budget components, but more likely by the modified response of the model vegetation to the decrease in available energy. This modified response of the model vegetation to the lower net radiation was also observed with unchanged vegetation, that is, when the same parameter values for the physiological control as in LU19 are used (experiment M-S). The altered

response of the model vegetation is only possible because the water availability in the study area is, despite the drainage of large areas, still high.

Changes in the extent of the forested areas proved to be an important factor for the changes in the regional climate, where regional refers to an area of equal to or more than 10^4 km^2 (see, e.g., Cleugh et al., 2004; Kustas et al., 2003). During the daytime, afforestation led to a distinct average warming, whereas deforestation had a considerable cooling effect, especially in areas where the percentage of deforestation was high. The observed cooling effect of deforested areas on the near-surface temperature is in good agreement with other studies that investigated the effect of historical land-cover changes on a continental to global scale (Bonan, 1997; Brovkin et al., 1999; Govindasamy et al., 2001; Bounoua et al., 2002).

During the night, a substantial cooling on the low-lying plains was caused by the land-use changes. This is in good agreement with Venäläinen et al. (Venäläinen et al., 1999), who showed that the peatland draining with subsequent afforestation in Finland had lowered the nighttime minimum temperatures. This was mainly caused by the change in the soil heat flux. However, in their study they only allowed changes in the surface and soil properties. They concluded that changes in the surface properties (shortwave albedo, longwave emissivity, surface roughness) had only a minor influence on the near-surface temperatures. In contrast to the study by Venäläinen et al. (Venäläinen et al., 1999), our sensitivity analyses showed that changes in the physiological properties were even more important than changes in the soil heat flux caused by altered soil properties. Thus, the inclusion of changes in the physiological properties due to land-use changes proves to be a very important factor for future assessments of the impact of land-use changes on the regional climate. The vegetation canopy under present conditions is distinctly warmer, thus leading to an enhanced loss of longwave radiation during calm and clear nights. Furthermore, simulated changes in the ground heat flux during the night were mainly caused by cooler ground conditions, which developed due to the changed morphological and physiological properties during the day. Hence, changes in the vegetation cover indirectly affected the soil heat flux at night, indicating a memory effect of the soil that lasts for several hours.

As the changes in the physiological properties were an important factor for the changes in the near-surface atmospheric conditions, the question arises whether the physiological module was able to represent the historical conditions correctly. In the case of wetland- or bog-cover types, a more detailed surface evaporation module including a moss layer could possibly have improved the results. However, the benefit of a separate moss layer to simulate the surface evaporation must be assumed to be rather small under clear-sky conditions in summer: the soil surface rather rapidly dries up and hence does not contribute much to the total evapotranspiration. Thus, we think that the big-leaf–big-stoma approach in combination with the simple first-order approach to model the additional soil surface evaporation also adequately represented the past conditions.

Regarding the convective activity over the simulated days, the thermodynamic potential for deep convection is nowadays increased. Since the simulated days were cloud free, the impact of the historical land-use changes on the precipitation amount could not be investigated. Therefore, longer simulations including periods with precipitation must be carried out in a future study. From the findings presented

here, it can be deduced that the historical land-use changes most likely have led to more cumulus convective rainfall during the summertime.

The evaporation–cloud–radiation feedback is still a very challenging issue in the context of regional climate modeling (e.g., Denning et al., 2003). With our choice of clear-sky days, we aimed at excluding the uncertainty in the representation of these feedback processes in present regional climate models. However, in future studies dealing with longer time periods, the impact of the land-use changes on cloud formation will certainly have to be included.

The observed changes in the near-surface temperature due to the historical land-use changes are opposite to temperature changes associated with global-scale greenhouse gas concentration increases, but they qualitatively agree with global-scale land-use change effects that were presented in the Intergovernmental Panel on Climate Change (IPCC; Houghton et al., 2001) report. Quantitatively, the daily average temperature on these typical summer days decreased by up to 0.3°C due to the JGK. The average difference in the net radiation (LU20 – LU19) over the 2 days is –6.3 W m^{-2}, which is high compared to the global annual-mean radiative forcing of –0.2 W m^{-2} associated with land-use changes (albedo) during the period from the preindustrial era (1750) to the present (about 2000; Houghton et al., 2001).

Although it is not encouraged to extrapolate the results of this short-term simulation to the long-term climate, it can be qualitatively argued that on the regional scale the projected increase in surface air temperatures due to increasing greenhouse gas concentrations was to some extent lowered or even masked by the opposite effects resulting from land-use changes. The documented historical land-use changes on the Swiss Plateau also had a contrary effect on the diurnal temperature range and the daily minimum and maximum temperatures compared to those expected for the future climate change. Due to the JGK, the nighttime minimum temperature decreased more than did the daytime maximum temperature, hence, increasing the diurnal temperature range. Future projections of the climate (Houghton et al., 2001), however, expect a decrease in the diurnal temperature range due to a greater increase of the nighttime minimum temperatures as compared to the daytime maximum temperatures. This shows the necessity to include the forcings of land-use changes in the scenarios for future climate predictions.

7. Conclusions

In qualitative agreement with previous findings (see Houghton et al., 2001), our numerical simulations showed a cooling effect due to the historical land-use changes: daily average near-surface temperatures during the typical summer days decreased by up to 0.3°C, with a most prominent cooling of up to 0.6°C at the end of the night in the atmospheric surface layer on the low-lying plains. During the day, the various types of land-use conversions led to spatially inhomogeneous changes in the air temperature. Deforested areas showed a cooling of up to 2.0°C, whereas afforested areas produced a warming effect of up to 1.0°C. The most frequent land-use conversion from bog to croplands showed only a weak cooling tendency during the day. In contrast, the nighttime cooling was more pronounced

and clearly restricted to the low-lying plains where most of the blanket bog area was converted to croplands. In addition, historical land-use changes increased the daytime average water vapor mixing ratio by up to 0.2 g kg^{-1}.

The sensitivity experiments revealed that during the day changes in the morphological properties explained most of the temperature and humidity changes in the atmosphere. The increase of the average albedo reduced the net radiation at the surface by up to 30 W m^{-2}. This in turn led to a modified physiological control of the vegetation, which resulted in an altered partitioning of the incoming energy into sensible and latent heat toward a lower Bowen ratio. During the night, changes in the physiological properties of the vegetation cover led to a modified thermal regime within the canopy. Thus, physiological control over regional climate was revealed to be one of the key factors in our investigation.

A follow-up of this work is planned to carry out longer simulations of 1 month that include more of the climatologically relevant weather conditions observed in the study area.

Acknowledgments. This work was carried out as part of the IGBP/IHDP project on Land Use and Land Cover Changes (LUCC). NS was funded by the Swiss KTI Grant 4136.1 and by the Swiss National Science Foundation Grant 21-66927.01. WE was funded by a Hans Sigrist Fellowship grant of the University of Bern. The authors wish to acknowledge use of the Ferret program for analysis and graphics in this paper. Ferret is a product of NOAA's Pacific Marine Environmental Laboratory.

References

Apsley, D. D., and I. P. Castro, 1997: A limited-length-scale k–ε model for the neutral and stably-stratified atmospheric boundary layer. *Bound.-Layer Meteor.,* **83,** 75–98.

Bonan, G. B., 1997: Effects of land use on the climate of the United States. *Climatic Change,* **37,** 449–486.

Bounoua, L., R. Defries, G. J. Collatz, P. Sellers, and H. Khan, 2002: Effects of land cover conversion on surface climate. *Climatic Change,* **52,** 29–64.

Brovkin, V., A. Ganopolski, M. Claussen, C. Kubatzki, and V. Petoukhov, 1999: Modelling climate response to historical land cover change. *Global Ecol. Biol.,* **8,** 509–517.

Chase, T. N., R. A. Pielke, T. G. F. Kittel, M. Zhao, A. J. Pitman, S. W. Running, and R. R. Nemani, 2001: Relative climatic effects of landcover change and elevated carbon dioxide combined with aerosols: A comparison of model results and observations. *J. Geophys. Res.,* **106,** 31 685–31 691.

Clappier, A., 1998: A correction method for use in multidimensional time-splitting advection algorithms: Application to two- and three-dimensional transport. *Mon. Wea. Rev.,* **126,** 232–242.

Cleugh, H. A., M. R. Raupach, P. R. Briggs, and P. A. Coppin, 2004: Regional-scale heat and water vapour fluxes in an agricultural landscape: An evaluation of CBL budget methods at oasis. *Bound.-Layer Meteor.,* **110,** 99–137.

Colella, P., and P. R. Woodward, 1984: The piecewise parabolic method (PPM) for gas-dynamical simulations. *J. Comput. Phys.,* **54,** 174–201.

Deardorff, J., 1978: Efficient prediction of ground surface temperature and moisture, with inclusion of a layer of vegetation. *J. Geophys. Res.,* **83,** 1889–1903.

Denning, A. S., M. Nicholls, L. Prihodko, I. Baker, P.-L. Vidale, K. Davis, and P. Bakwin,

2003: Simulated variations in atmospheric CO_2 over a Wisconsin forest using a coupled ecosystem–atmosphere model. *Global Change Biol.,* **9,** 1241–1250.

Eugster, W., and Coauthors, 1998: Spatial variation of annual nitrogen deposition in a rural region in Switzerland. *Environ. Pollut.,* **102,** 327–355.

Galler, J. J., T. S. Bianchi, M. A. Alison, L. A. Wysocki, and R. Campanella, 2003: Biogeochemical implications of levee confinement in the lowermost Mississippi River. *Eos, Trans. Amer. Geophys. Union,* **84,** 469–476.

Govindasamy, B., P. B. Duffy, and K. Caldeira, 2001: Land use changes and Northern Hemisphere cooling. *Geophys. Res. Lett.,* **28,** 291–294.

Houghton, J. T., Y. Ding, D.J. Griggs, M. Noguer, P.J. van der Linden, X. Dai, K. Maskell, and C.A. Johnson, Eds., 2001: *Climate Change 2001: The Scientific Basis*. Cambridge University Press, 881 pp.

Kalnay, E., and Coauthors, 1996: The NCEP/NCAR 40-Year Reanalysis Project. *Bull. Amer. Meteor. Soc.,* **77,** 437–471.

Kistler, R., and Coauthors, 2001: The NCEP–NCAR 50-year reanalysis: Monthly means CD-ROM and documentation. *Bull. Amer. Meteor. Soc.,* **82,** 247–267.

Kustas, W. P., T. J. Jackson, J. H. Prueger, J. L. Hatfield, and M. C. Anderson, 2003: Remote sensing field experiments evaluate retrieval algorithms and land-atmosphere modeling. *Eos, Trans. Amer. Geophys. Union,* **84,** 485–493.

Loveland, T. R., B. C. Reed, J. F. Brown, D. O. Ohlen, J. Zhu, L. Yang, and J. W. Merchant, 2000: Development of a global land cover characteristics database and IGBP DISCover from 1-km AVHRR data. *Int. J. Remote Sens.,* **21,** 1303–1330.

Mölders, N., 1999: On the effects of different flooding stages of the Oder and different land-use types on the distributions of evapotranspiration, cloudiness and rainfall in the Brandenburg–Polish border area. *Contrib. Atmos. Phys.,* **72,** 1–25.

———, 2000: Similarity of microclimate as simulated in response to landscapes of the 1930s and the 1980s. *J. Hydrometeor.,* **1,** 330–352.

Paltridge, G. W., and C. M. R. Platt, 1976: *Radiative Processes in Meteorology and Climatology*. Elsevier, 318 pp.

Perego, S., 1996: *Ein numerisches Modell zur Simulation von Sommersmog (G47)*. Geographica Bernensia, 202 pp.

———, 1999: Metphomod—A numerical mesoscale model for simulation of regional photosmog in complex terrain: Model description and application during Pollumet 1993 (Switzerland). *Meteor. Atmos. Phys.,* **70,** 43–69.

Peyer, K., 1985: Die Böden. *Gesamtmelioration Ins-Gampelen-Gals 1970–1985,* A. von Waldkirch, Ed., Kantonales Meliorationsamt, 7–9.

Pielke, R. A., 1984: *Mesoscale Meteorological Modeling*. Academic Press, 612 pp.

———, 2001: Influence of the spatial distribution of vegetation and soils on the prediction of cumulus convective rainfall. *Rev. Geophys.,* **39,** 151–177.

———, and R. Avissar, 1990: Influence of landscape structure on local and regional climate. *Landscape Ecol.,* **4,** 133–155.

Segal, M., R. W. Arritt, C. Clark, R. Rabin, and J. Brown, 1995: Scaling evaluation of the effect of surface characteristics on potential for deep convection over uniform terrain. *Mon. Wea. Rev.,* **123,** 383–400.

Siegrist, F. C., 2001: Determination of energy and trace gas fluxes on a regional scale. Ph.D. thesis, University of Bern, Institute of Geography, 113 pp.

Stohlgren, T. J., T. N. Chase, R. A. Pielke, T. G. F. Kittel, and J. S. Baron, 1998: Evidence that local land use practices influence regional climate, vegetation, and stream flow patterns in adjacent natural areas. *Global Change Biol.,* **4,** 495–504.

Venäläinen, A., L. Rontu, and R. Solantie, 1999: On the influence of peatland draining on local climate. *Boreal Environ. Res.,* **4,** 89–100.